MICROSTRUCTURE AND PALEOPIEZOMETRIC CONSTRAINTS ON DEFORMATION CONDITIONS OF OLIVINE FROM THE SOUTHERN APPALACHIAN BUCK CREEK ULTRAMAFIC COMPLEX

Grand Valley State University Geology Department

Session 96-9

***Benjamin Pummell (pummellb@mail.gvsu.edu), Ginny Peterson (petersvi@gvsu.edu)**, Geology Department, Grand Valley State University, Allendale, MI 49401*

Abstract:

Microstructural and paleopiezometric analyses help constrain conditions and mechanisms of deformation of the Buck Creek ultramafic complex in southwestern North Carolina. Previous work has determined that the complex is an emplaced fragment of partially subducted ocean crust that experienced anhydrous prograde metamorphic conditions to about 800˚C and 1.0 GPa. Twelve olivine-rich dunite/troctolite samples from the Buck Creek ultramafic complex are the focus of this study. Previous work with electron backscatter diffraction (EBSD) shows that the olivine crystallographic preferred orientation (CPO) patterns are generally consistent with axial-[100] or D-type fabric formed under moderate to high stresses with low water content. Axial fabrics may also result from non-plane strain conditions (e.g. constriction or flattening).

Textures and recrystallized grain size were determined using the petrographic microscope and deformation conditions were interpreted by comparison with experimental studies. The dominant olivine grain sizes range from 1.5 – 2.6 mm. Recrystallization textures include kink bands and subgrains, undulatory extinction, core-mantle structures, bulge-recrystallization, and encapsulated grains. Micro-inclusions of mineral grains (too small for microscopic ID) in some olivine locally appear to be oriented by the olivine crystal structure or along microcracks. One micro-inclusion appears to be twinned.

Average recrystallized grain and subgrain diameters (127 – 166 µm) are relatively consistent among the samples. Based on experimental work, recrystallized grain size can serve as a paleopiezometer and be used to estimate deformation mechanisms. The range of sizes are consistent with differential stress ranging from ~ 27 – 43 MPa (~ 33 MPa avg.). This can be related to deformation mechanisms of diffusion creep, dislocation creep, and/or grain boundary sliding, consistent with relatively high temperature deformation conditions. At 33 MPa, experimental work suggests that D-type fabrics form at ~ 1400 – 1500˚C. Integration of field and textural observations, paleopiezometry, and EBSD data may point to preservation of olivine deformation textures formed prior to crustal emplacement and deformation.

doi: 10.1130/abs/2018AM-321116

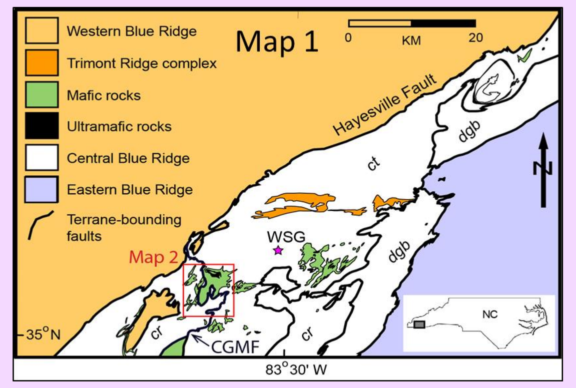

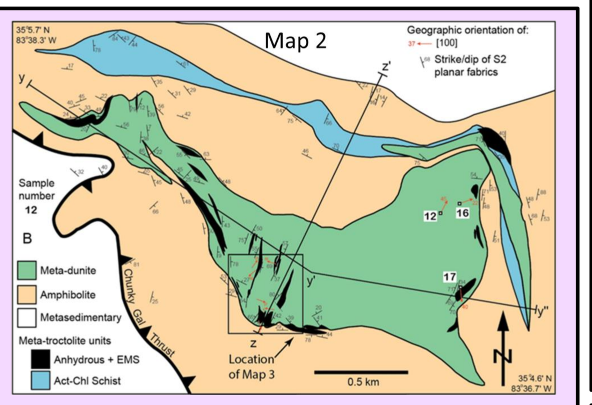

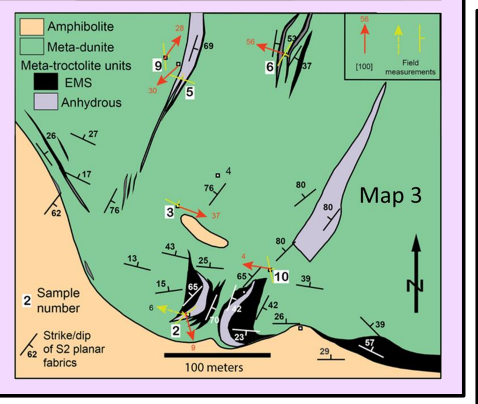

Map 1: Simplified geologic map of part of the Blue Ridge region (adapted from Peterson and Ryan, 2009). CGMF = Chunky Gal Mountain Fault; ct = Cartoogechaye terrane; cr = Cowrock terrane; dgb = Dahlongega Gold Belt; WSG = Winding Stair Gap. The Buck Creek Ultramafic Complex is highlighted.

Map 2: Simplified geologic map of the Buck Creek Ultramafic Complex. Sample locations are marked. EMS = Edenite-Margarite schist; Act/Chl = Actinolite/Chlorite.

Map 3: Closer view in the complex. More sample number locations are marked.

Synthetic Olivine Deformation

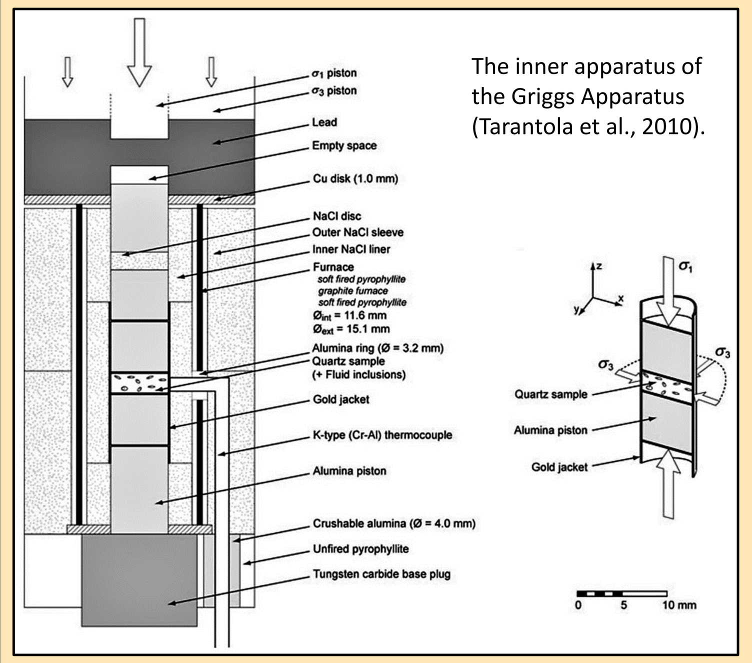

Polycrystalline and single crystal samples are used to simulate deformations closer to natural samples. Most approaches use pure powdered olivine (single/multiple grains). Some use natural unpurified crystals. Synthetic dunite is formed by heating the olivine sample in a pressurized cylinder. Talc is commonly used to introduce water to the dunite samples. Synthetic dunite slabs are deformed in the Griggs Apparatus or piston, which provides a single direction of shear (σ1) while maintaining a confining pressure around the sides (σ3). In some studies, the dunite slab is cut at different angles to give the sample rotational strain.

Acknowledgements:

The EBSD data presented in this poster was generated at the SEM/EBSD facility at Washington and Lee University and the EBSD work was supported by a Michigan Space Grant Consortium Seed Grant (to Peterson, 2016).

Full Thin-Section Photos

NC16-5

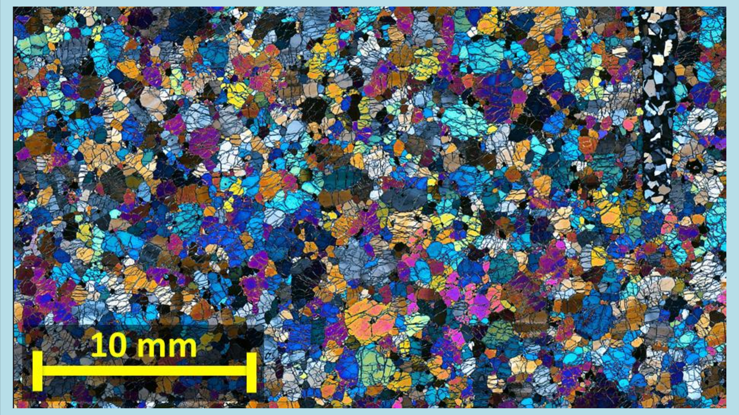

NC13-10

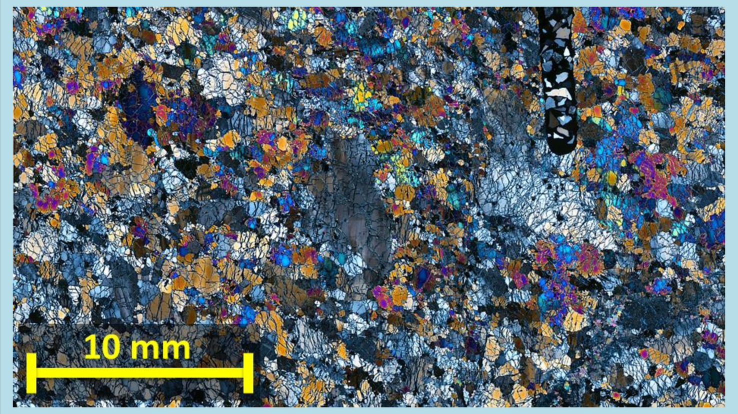

NC13-9B

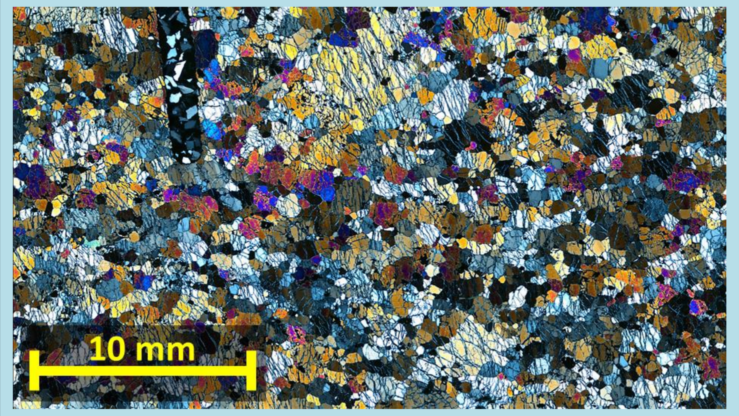

Buck Creek Microstructural Observations

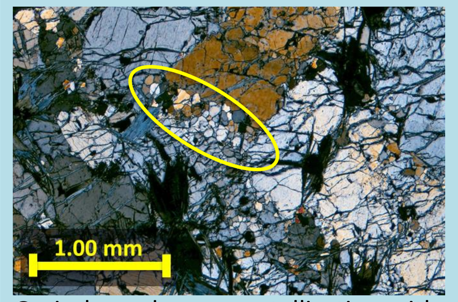

Grain-boundary recrystallization with chlorite alteration. Four-grain junctions are present (NC16-17).

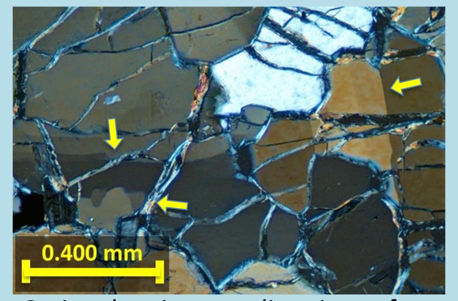

Grains showing two directions of kink banding. Subgrains are present (NC16-12).

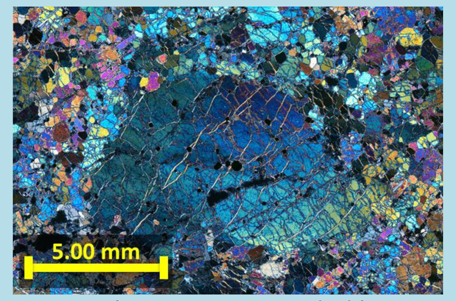

Large relict grain surrounded by recrystallized grains in core-mantle complex (NC16-3B).

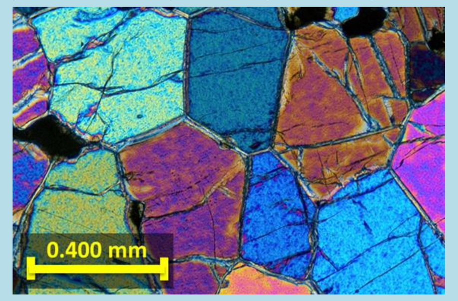

Annealed grains with 120˚ triple junctions (NC16-6A).

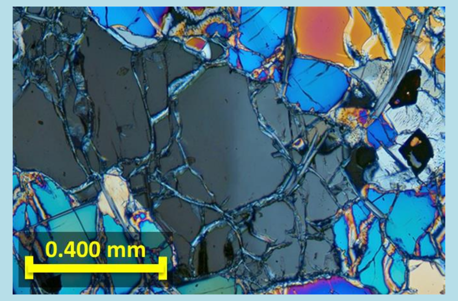

Undulose extinction is uncommon and occurs in larger grains (NC13-10).

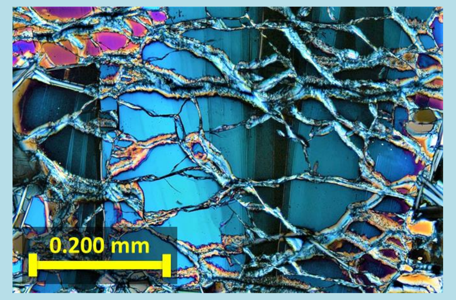

Kink banding in close orientation (NC13-10).

Mineral Micro-Inclusions

Thin section samples NC16-5, NC16-5A, NC16-5B, NC16-12, and NC16-17 show micro-inclusions. Originally thought to be fluid inclusions, this is falsifiable as signs of air pockets or fluid are not present and the inclusions go extinct. Inclusions are at times oriented within the olivine grains. Occurrence within the grains varies from forming along healed microcracks, kink band boundaries, to being more widespread throughout a grain. The composition of the mineral within the olivine is unknown.

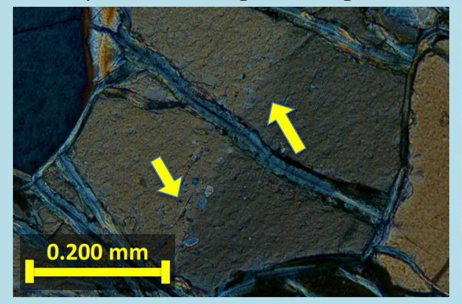

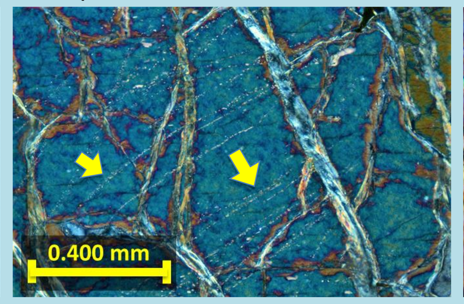

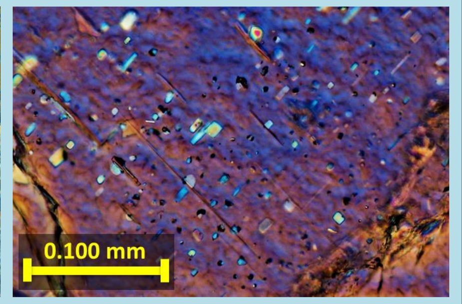

Synthetic Dunite Microstructures

Temperatures tend to remain high in such studies in the recrystallization properties of olivine, ranging from 1100˚C to 1300˚C. There are a few tests that go below that temperature to create a comparison. Microstructures in the synthetic and natural samples differ with conditions. Kink banding is also shown in many cases. Dynamic recrystallization is a common occurrence in sample along the boundaries of the relict grains. Higher temperatures show higher amounts of bulging "wet" samples show microstructures at lower temperatures and pressures.

Temperature (˚C)	σ (MPa)	CPO type	Wet or dry sample	Microstructural Comments
700 - 800	0-50	Axial-[010], B-type	Wet	Well developed foliation. Fine grained olivine with needle like Opx.
			Dry	Polygonal olivine grains with triple junctions.
800 - 900	0-50	Axial-[010], A-type	Wet	Fine grained olivine matrix with elongated large olivine grains. Triple and quadruple junctions are present. (2)
			Dry	Widely spaced subgrain boundaries perpendicular to foliation. Four grain junctions are present.
900 - 1000	0-50	Axial-[010], A-type, B-type, D-type	Dry	Grains are aligned obliquely to foliation. Larger grains show undulatory extinction. (3)
1000 - 1100	0-50	Axial-[010], A-type, D-type	Dry	Olivine grains contain two different orientations of subgrains. Subgrains are at a low angle/oblique to the foliation.
1100 - 1200	0-50	A-type, D-type	Dry	Grain boundaries and subgrain boundaries with other minerals are aligned. Grains have a diamond shape. No Melting.
	300-600		Wet	Fine grain recrystallization. New grains are devoid of deformation. Dislocation creep is rare.
1200 - 1300	100-300	Axial-[010], A-type	Dry	Dynamic Recrystallization is present. Relict grains are elongated towards the strain ellipsoid. Fine recrystallization.
			Wet	Fine grain recrystallization. New grains are devoid of deformation. Some trace melt.
	600-1000		Dry	Porphyroclastic texture. Highly recrystallized. Flattened relict grains. Intragranular recrystallization is present (5).
	>1000		Dry	Very distinct kink banding. Recrystallization along kink band boundaries.
1300 - 1400	50-100	Axial-[010], A-type, D-type	Dry	Foliation is well defined. Undulose extinction is in most grains. Fine recrystallization. (4,6)
			Wet	Large amounts of recrystallization. Fine recrystallization. Some trace melt. (6)
	600-1000		Dry	Very fine recrystallization around porphyroclasts

1.

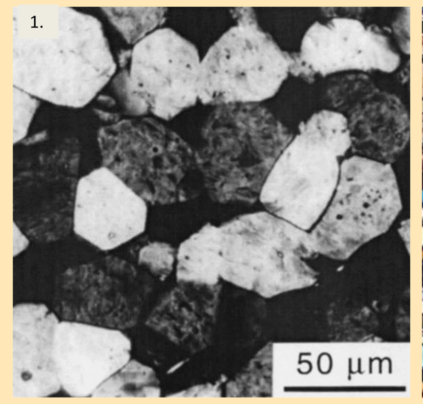

Image from Zhang et al. (2000) shows the synthetic olivine aggregate after the initial annealing process at 1300˚C at confining pressures of 300 MPa. Crystal faces are straight with 120˚ triple points. Grains are of nearly equal sizes.

2.

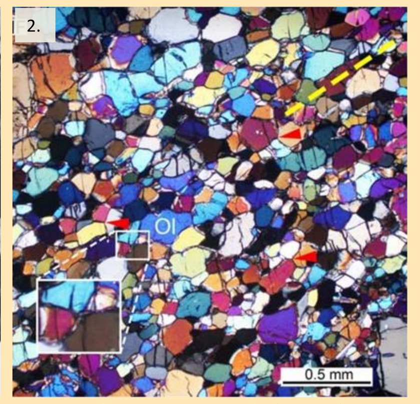

Image from Cao et al. (2017) shows a "wet" sample. This is a natural sample that is calculated to have had equilibrium temperatures of 825˚C with differential stresses of 27 MPa. Foliation is given by the dashed yellow line and a four-grain junction is shown.

3.

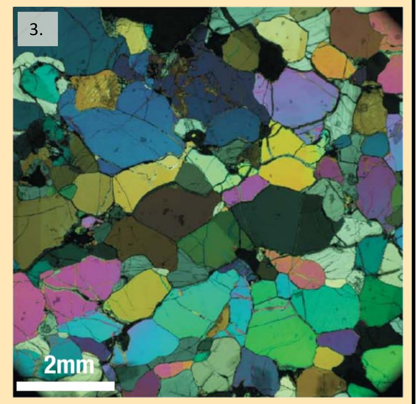

Natural dunite sample from Chatzaras et al. (2016) showing a "dry" sample at 939˚C and 40 MPa. Foliation is less noticeable in this sample. Subgrain boundaries are oblique to foliation.

4.

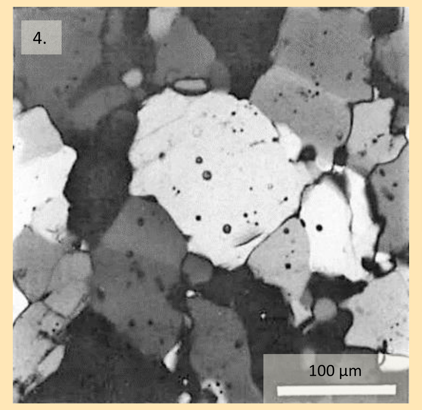

Image from Karato (1988) showing small-scale boundary recrystallization and multiple directions of subgrain boundaries. Conditions are at 1300˚C and 63 MPa for this sample.

5.

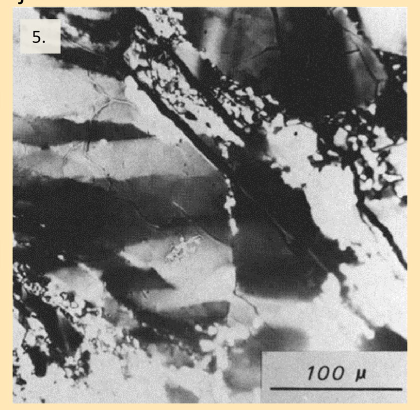

Image from Zeuch and Green II (1984) showing distinct subgrains and kink banding at 1200˚C and 640 MPa. Dynamic recrystallization can be found along grain boundaries and in intragranular microcracks.

6.

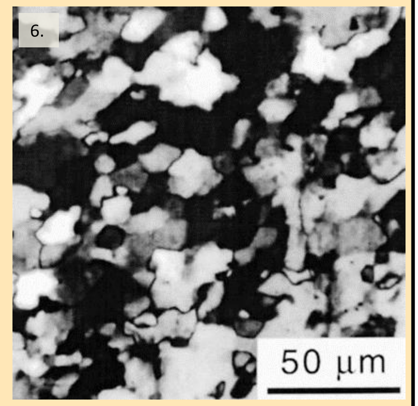

Heavily recrystallized sample from Zhang et al. (2000). Foliation direction is evident. Conditions for this sample are 1300˚C and 100 MPa. Wet conditions produce grain sizes slightly smaller than this.

Buck Creek Paleopiezometry

Paleopiezometric data was collected from twelve thin sections. Both subgrains and recrystallized grains were measured. Diameter measurement includes subgrains as well kink band boundaries. Recrystallized grains were chosen by observing their relative extinction to their parent grain. Patchy extinction and alignment of microfractures allowed for the recognition of these grains. These grains contain little to no ductile deformation. The figure from sample NC16 – 3 shown below shows this recrystallization.

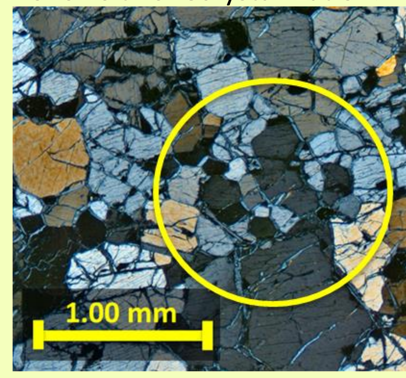

One hundred subgrains ranging in origin from kink banding, subgrain rotation, grain-boundary recrystallization, and bulge recrystallization were measured at random in each thin-section. Grain size is able to be calculated from the following equation.

$$D_g = A\sigma^{-n}$$

Given that in the Buck Creek thin sections that the grain size diameter, D_g, is known but the differential stress, **σ**, is unknown, the equation must be rewritten. The new adjusted equation is shown below.

$$\sigma = (D_g/A)^{-(1/n)}$$

In both equations, variables **A** and **n** are empirically derived constants. Values for these variables in each equation used is given in the plot below according to the source.

The average grain size throughout all the thin sections is 142.89µm. Using the listed equations, the differential stress ranges from 30.30 – 36.60MPa. Data from the ImageJ method is plotted on the graph below. Differential stress results from this method were smaller than the microscope measurements.

Sample	Grain Size (µm)	Karato et al. (1980) formula (MPa)	Ross et al. (2000) formula (MPa)	Van der Wal (1993) formula (MPa)	Mercier (1977) formula (MPa)
NC16-3	166.03	27.53	32.29	29.55	26.62
NC16-3A	149.98	30.00	34.98	31.90	28.91
NC16-3B	151.74	29.71	34.66	31.62	28.64
NC16-5	142.90	31.26	36.34	33.08	30.07
NC16-5A	144.14	31.03	36.09	32.87	29.86
NC16-5B	151.29	29.78	34.74	31.69	28.71
NC16-6A	140.07	31.79	36.92	33.58	30.56
NC13-9B	162.41	28.04	32.86	30.05	27.10
NC13-10	114.99	37.58	43.12	38.95	35.88
NC16-12	130.94	33.66	38.93	35.33	32.28
NC16-16	133.15	33.19	38.42	34.89	31.85
NC16-17	127.07	34.53	39.86	36.14	33.08
Averages	142.89	31.51	36.60	33.30	30.30

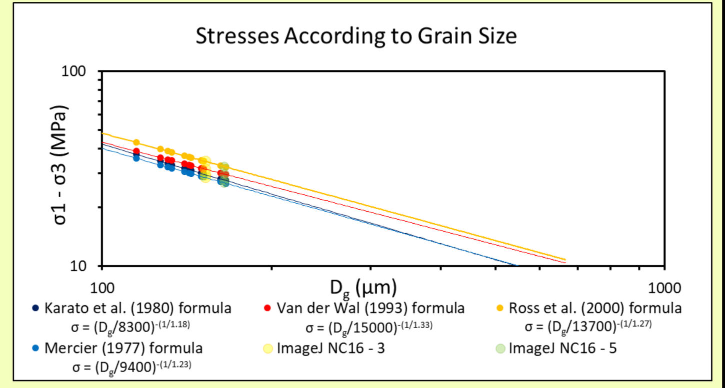

ImageJ Paleopiezometry Method

NC16 - 5

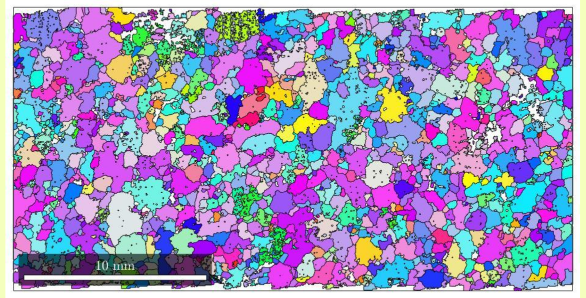

NC16 - 3

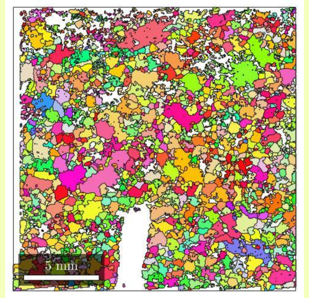

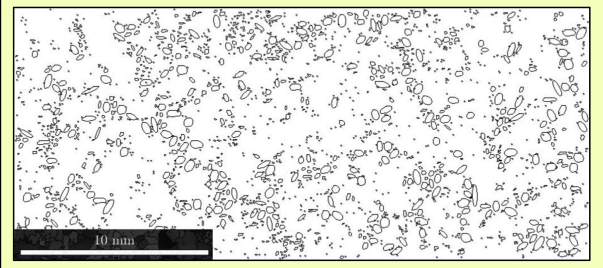

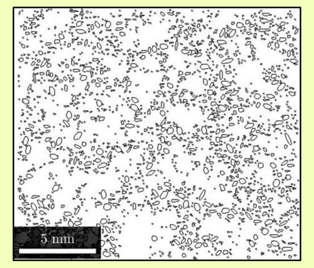

Previous work by VanEss and Peterson (2018) used the program ImageJ and grain maps generated with EBSD analysis (left) to estimate grain size and shape for strain analysis. Here, we explore the same approach to compare to thin section estimates of grain size. The EBSD grains were first filtered by area to slightly exceed the grain size range observed in thin section. The line of no finite elongation (LNFE) was then calculated as the diameter. The grain size range from this approach matched thin section measurements. Limitations with this method include the program selecting all grains in the selected range. This includes grains that are not subgrains as well as void spaces and pockets of other minerals. A next step will be to analyze EBSD data to estimate grain size.

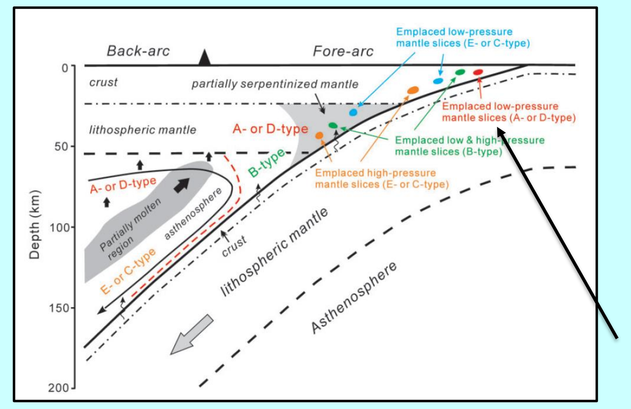

Tectonic setting

Schematic illustration from Cao et al. (2015) Figure 19b showing olivine fabric distributions in a subduction zone setting - mature and cool mantle wedge.

The diagram shows possible subduction zone settings for D-type fabrics – both *in situ* (original mantle fabrics) or *ex situ* (may be original fabric or acquired during emplacement/exhumation).

The *ex situ* setting could be similar to that for the Buck Creek dunite.

Integration with EBSD analysis of Buck Creek Olivine samples

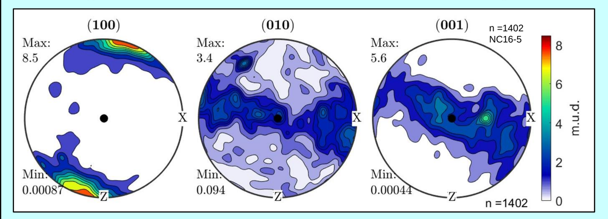

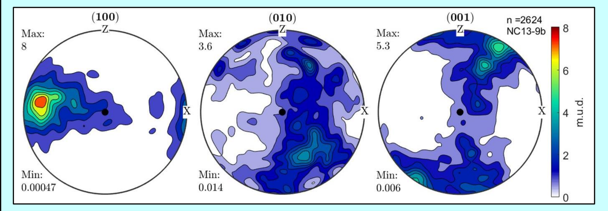

EBSD analyses of Olivine from several Buck Creek samples (DeYoung et al. 2017) produce CPO (Crystallization Preferred Orientation) diagrams consistent with D-type deformation fabrics – these are characterized by strong (100) clusters and girdles in (010) and (001) and [100] (0kl) slip system. Examples at left show these patterns. Challenges with identifying foliation/lineation in these samples resulted in unusual orientations for these plots. Efforts to better constrain the strain reference frame through analysis of the shape fabric (VanEss and Peterson, 2018) use of EBSD data to identify the Bulk Crystallographic Vorticity Axis have increased confidence in a D-type fabric interpretation.

Interpretation of D-type fabrics

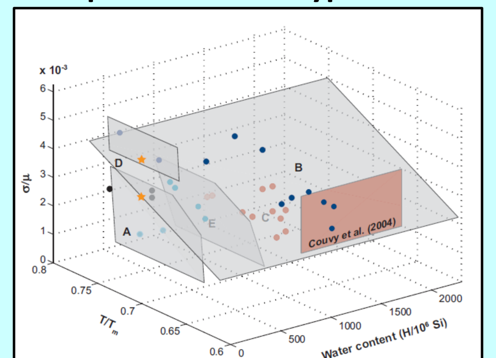

Figure 6 from Karato et al. (2008) (at left) showing the influences of temperature, stress, and water content on olivine CPO fabrics. D-type fabrics have generally been interpreted to indicate dislocation creep under relatively dry, high stress, and relatively low Temperature conditions.

Several studies (Hansen et al., 2014; Cao et al., 2015; Chatzeras et al., 2016) indicate that D-type fabrics can form in a range of deformation conditions and that both D- and A-type fabrics may form in response to similar deformation mechanisms and processes. Progressive strain favoring specific slip planes may determine which fabric forms.

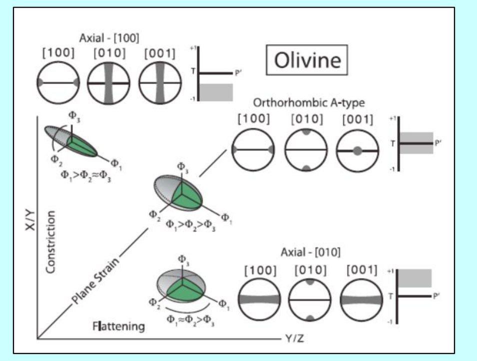

Figure 15 from Chatzeras et al. (2016) (at right) showing the relationship between finite strain geometry and olivine CPO symmetry. In naturally deformed samples Chateras et al. (2016) observe that D-type fabrics are associated with constructional strain (transtension). This is consistent with numerical models by Tommasi et al. (1999) that produce D-type fabrics in response to thickening-narrowing shear (classical transtension).

Interpretation Of Stress Data

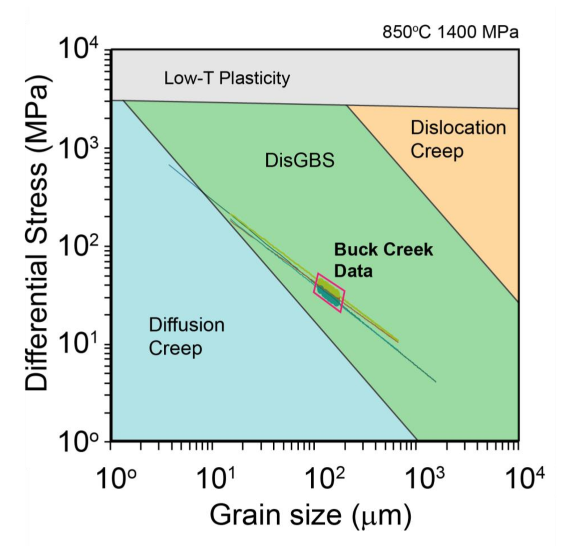

Olivine deformation mechanism map (above) adapted from Chatzaras et al. (2016) Figure 11 with Buck Creek Grain size-Stress data. Increasing temperatures and pressures narrow the DisGBS (Dislocation accommodated Grain-Boundary Sliding) field.

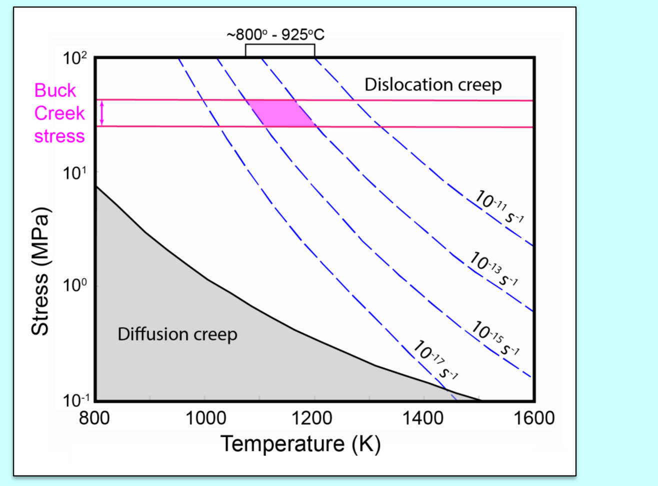

Olivine deformation map (above) with strain rates adapted from Cao et al. (2015) Figure 17 – generated using olivine flow laws for dry conditions at P=1.5 Gpa. Buck Creek stress estimates superimposed with shaded magenta representing range of typical mantle strain rates (10^{-13} – 10^{-15}).

Buck Creek Metatroctolite/Dunite peak metamorphic conditions ~850°C, 1.0-1.4 GPa (anhydrous)

Conclusions

- Buck Creek Olivine Microstructures give evidence for both Dislocation Creep and DisGBS.
- Paleopiezometric results from Buck Creek samples are similar to published data (Chatzaras et al., 2016) from natural samples and fall in the DisGBS field.
- Paleopiezometric results from Buck Creek samples suggest temperatures similar to thermo-barometric estimates for peak metamorphic conditions previously determined for the Buck Creek complex.
- Recent studies indicate that D-type CPO fabrics can form under variable conditions and mechanisms. Thus, the relatively low stress conditions determined for these Buck Creek samples are consistent with interpretations of D-type CPO patterns.

References Cited:

Cao, Y., Jung, H., Song, S., Park, M., Jung, S. and Lee, J., 2015. Plastic deformation and seismic properties in fore-arc mantles: a petrofabric analysis of the Yushigou Harzburgites, North Qilian Suture Zone, NW China. *Journal of Petrology*, *56*(10), pp. 1897–1944.

Cao, Y., Jung, H., and Song, S., 2017, Olivine fabrics and tectonic evolution of fore-arc mantles: A natural perspective from the Songshugou dunite and harzburgite in the Qinling orogenic belt, central China: Geochemistry, Geophysics, Geosystems, v. 18, p. 907–934, doi:10.1002/2016GC006614.

Chatzaras, V., Kruckenberg, S.C., Cohen, S.H., Medaris Jr., L.G., Withers, A.C., and Bagley, B., 2016, Axial-type olivine crystallographic preferred orientations: The effect of strain geometry on mantle texture: Journal of Geophysical Research: Solid Earth, v. 121, p. 4895–4922, doi:10.1002/2015JB012628.

Chopra, P.N., 1986, The plasticity of some fine-grained aggregates of olivine at high pressure and temperature: Mineral and Rock Deformation: Laboratory Studies, v. 36, p. 25–33.

DeYoung, S.M., Peterson, V.L., Rahl, J.M., 2017, Using Olivine LPO and misorientation analysis to constrain deformation and emplacement conditions of the Buck Creek ultramafic complex, Blue Ridge province, North Carolina. Geological Society of America, Southeastern Section *Abstracts with Programs*.

Hansen, L.N., Zhao, Y.H., Zimmerman, M.E. and Kohlstedt, D.L., 2014. Protracted fabric evolution in olivine: Implications for the relationship among strain, crystallographic fabric, and seismic anisotropy: Earth and Planetary Science Letters, *v. 387*, p. 157–168.

Karato, S., Jung, H., Katayama, I., and Skemer, P., 2008, Geodynamic Significance of Seismic Anisotropy of the Upper Mantle: New Insights from Laboratory Studies: Annual Review of Earth and Planetary Sciences, v. 36, p. 59–95, doi: 10.1146/annurev.earth.36.031207.124120.

Karato, S., Toriumi, M., and Fujii, T., 1980, Dynamic recrystallization of single olivine crystals during high-temperature creep: Geophysical Research Letters, v. 7, no. 9, p. 649–652.

Mercier., J.C.C., 1977, Natural Peridotites: Chemical and Rheological Heterogeneity of the Upper Mantle, Ph.D. Thesis, SUNY, Stone Brooke, N.Y., p. 668.

Peterson, V., and Ryan, J.G., 2008, Petrogenesis and structure of the Buck Creek mafic-ultramafic suite, southern Appalachians: Constraints on the ophiolite evolution and emplacement in collisional orogens: GSA Bulletin, v. 121, no. 3, p. 615–629, doi:10.1130/B26302.1.

Ross, J.V., Lallemant, H.G.A., and Carter, N.L., 1980, Stress dependence or recrystallized grains and subgrains in olivine: Tectonophysics, v. 70, p. 39–61.

Tarantola, A., Diamond, L.W., and Stünitz H., 2010, Modification of fluid inclusions in quartz by deviatoric stress I: experimentally induced changes in inclusion shapes and microstructures: Contributions to Mineralogy and Petrology, v. 160, no. 6, p. 825–843, doi: 10.1007/s00410-010-0509-z.

Tommasi, A., B. Tikoff, and A. Vauchez (1999), Upper mantle tectonics: Three-dimensional deformation, olivine crystallographic fabrics and seismic properties, Earth Planet. Sci. Lett., v. 168, p. 173–186, doi:10.1016/S0012-821X(99)00046-1.

VanEss, J., Peterson, V.L., 2018, Exploring methods to determine the strain ellipsoid in dunites to interpret EBSD patterns. Geological Society of America, North Central Section *Abstracts with Programs*, Vol. 50, No. 4, doi: 10.1130/abs/2018NC-311977.

Van der Wal, D., Chopra, P., Drury, M., and Fitz Gerald, J., 1993, Relationships between dynamically recrystallized grain size and deformation in experimentally deformed olivine rocks: Geophysical Research Letters, v. 20, no. 14, p. 1479–1482.

Zeuch, D. H., and Green II, H. W., 1984, Experimental deformation of a synthetic dunite at high temperature and pressure. 1. Mechanical behavior. Optical microstructure and deformation mechanism, Tectonophysics, v. 110, p. 233–262.

Zhang, S., Karato, S., Gerald, J. F., Faul, U. H., and Zhou, Y., 2000, Simple shear deformation of olivine aggregates, Tectonophysics, v. 316, p. 133–152.